Solar Energy 157 (2017) 603–613

Contents lists available at ScienceDirect

Solar Energy

journal homepage: www.elsevier.com/locate/solener

Addressing the impact of rear surface passivation mechanisms on ultra-thin $Cu(In,Ga)Se_2$ solar cell performances using SCAPS 1-D model

R. Kotipalli[a,*], O. Poncelet[a], G. Li[a,b], Y. Zeng[b], L.A. Francis[a], B. Vermang[c,d], D. Flandre[a]

[a] ICTEAM, Université catholique de Louvain, Louvain-la-Neuve 1348, Belgium
[b] School of Physics and Electronics, Hunan University, Changsha 410082, China
[c] Faculty of Engineering Technology, University of Hasselt, Hasselt 3500, Belgium
[d] IMEC, Kapeldreef 75, Leuven 3001, Belgium

ABSTRACT

We present a (1-D) SCAPS device model to address the following: (i) the surface passivation mechanisms (i.e. field-effect and chemical), (ii) their impact on the CIGS solar cell performance for varying CIGS absorber thickness, (iii) the importance of fixed charge type (+/−) and densities of fixed and interface trap charges, and (iv) the reasons for discrete gains in the experimental cell efficiencies (previously reported) for varying CIGS absorber thickness. First, to obtain a reliable device model, the proposed set of parameters is validated for both field-effect (due to fixed charges) and chemical passivation (due to interface traps) using a simple M-I-S test structure and experimentally extracted values (previously reported) into the SCAPS simulator. Next, we provide figures of merits without any significant loss in the solar cell performances for minimum net $-Q_f$ and maximum acceptable limit for D_{it}, found to be $\sim 5 \times 10^{12}\,cm^{-2}$ and $\sim 1 \times 10^{13}\,cm^{-2}\,eV^{-1}$ respectively. We next show that the influence of negative fixed charges in the rear passivation layer (i.e. field-effect passivation) is more predominant than that of the positive fixed charges (i.e. counter-field effect) especially while considering ultra-thin ($< 0.5\,\mu m$) absorber layers. Furthermore, we show the importance of rear reflectance on the short-circuit photocurrent densities while scaling down the CIGS absorber layers below 0.5 µm under interface chemical and field-effect passivation mechanisms. Finally, we provide the optimal rear passivation layer parameters for efficiencies greater than 20% with ultra-thin CIGS absorber thickness ($< 0.5\,\mu m$). Based on these simulation results, we confirm that a negatively charged rear surface passivation with nano-point contact approach is efficient for the enhancement of cell performances, especially while scaling down the absorber thickness below 0.5 µm.

1. Introduction

Thin-film (TF) solar cells have the potential for low-cost and large-scale photovoltaic deployment (Reinhard et al., 2013; Kaelin et al., 2004). Most recently, Centre for Solar Energy and Hydrogen Research Baden-Württemberg (ZSW-Germany) achieved impressive small-area ($0.5\,cm^2$) cell efficiencies (η) of 22.6%, surpassing the previous world record of 22.3% set by the Japanese $Cu(In,Ga)Se_2$ (CIGS) producer Solar Frontier (Jackson et al., 2016; Press release, 2015). On the other hand, this is a level not yet surpassed by any other thin-film or multi-crystalline silicon technology (Deng et al., 2015). However, the large-area world record of CIGS module lies at 17.5%, which is below the average 21.1% traditional photovoltaics (PV) modules Press release, 2016. In terms of manufacturing costs, CIGS modules can be developed for around $0.40–0.50/$W_p$, and the global annual production capacity currently stands at 2 GW. However, it is widely expected that CIGS TF PV production costs can be brought down to $0.25–0.30/$W_p$ and the module efficiency can be brought up to around 18% (Edoff et al., 2011; Dhere, 2007).

Current approaches and future priorities within CIGS research is focused on: (i) interface passivation (i.e. to reduce electronic recombination), (ii) absorber thickness-reduction (i.e. to reduce material usage), and (iii) highly reflective rear-surface (for enhanced rear-reflection). These approaches involve novel methods to passivate the front and rear surfaces of the CIGS absorber films by implementing (a) alkali post-deposition treatments to passivate the front CdS/CIGS interface defects (Jackson et al., 2016, 2014; Chirilă et al., 2013), (ii) front and rear surface passivation using gallium grading schemes (i.e. by introducing conduction band-gap widening effects) within the CIGS absorbers (Kotipalli et al., 2015; Gloeckler and Sites, 2005; Dullweber et al., 2001, 2000; Gabor et al., 1996; Lundberg et al., 2005, 2003; Dullweber et al., 2001;), and (c) electrical passivation of the CIGS/Mo-

---

* Corresponding author.
E-mail address: raja.kotipalli@uclouvain.be (R. Kotipalli).

http://dx.doi.org/10.1016/j.solener.2017.08.055
Received 23 December 2016; Received in revised form 9 August 2017; Accepted 18 August 2017

interface using a dielectric layer with point-contact approach (Vermang et al., 2014, 2013, 2014a, 2014b).

Amongst these approaches, gallium-grading schemes are the most commonly employed techniques within the CIGS PV community. Depending on the Ga grading concentration and profile, one can create and alter the built-in electric (E) field within the bulk of CIGS TF devices. The electric-field creation/modification is mainly attributed to the reformed position (relative) of the conduction-band edge with respect to the vacuum level (i.e. bandgap engineering) (Kotipalli et al., 2015; Gloeckler and Sites, 2005; Dullweber et al., 2001, 2000). In principle, it is possible to implement effective E-fields by tailoring either the bandgap and/or the doping profiles within the absorber films (Kotipalli et al., 2015; Gloeckler and Sites, 2005). In the former case, i.e. in the case of bandgap engineering towards the rear (CIGS/Mo back-contact), one can create an up-stream (shielding-barrier) for the minority carriers (electrons) not to be recombined at the surfaces (i.e. reducing the surface recombination rate at the CIGS/Mo-interface). This grading scheme and surface passivation methodology has proven to be successful for standard thickness (2–3 µm) CIGS absorber layers (Lundberg et al., 2003).

Next, the concept of rear-surface passivation using a dielectric layer with the point-contact approach is based on the c-Si passivated emitter rear cell (PERC) technology with efficiencies above 25% (Blakers et al., 1989; Green, 2015; Metz and et al., 2014; Zhao et al., 1998). The commonly employed dielectric passivation layers include thermally grown silicon dioxide (SiO_2), plasma-enhanced chemical vapor deposited (PECVD) silicon dioxide (SiO_x), and silicon nitride (SiN_x) Kotipalli et al., 2013. However, in recent years, amorphous aluminum oxide (Al_2O_3) deposited by industrial Atomic-layer-deposited (ALD) reactors (batch, spatial, or roll-to-roll) have emerged as an excellent rear surface passivation material for p-type PERC cell technologies (Hoex et al., 2008; Schmidt et al., 2008). This is principally due to the presence of a high density of negative fixed charges ($-Q_f$ $\sim 10^{12}$–$10^{13}\,cm^{-2}$) in combination with low interface states ($D_{it} \sim 10^{11}$–$10^{12}\,eV^{-1}\,cm^{-2}$), resulting in overall Surface Recombination Velocities (SRV) < 5 cm/s on high-quality p-type monocrystalline silicon surfaces (Kotipalli et al., 2013; Hoex et al., 2008; Schmidt et al., 2008). Owing to these capabilities on p-type surfaces, it has previously been seen that introducing ALD–Al_2O_3 surface passivation layer at the rear CIGS/Mo-interface can significantly improve cell efficiency, i.e. by more than 4.5% (abs.) Vermang et al., 2014. Additionally, the rear surface recombination rate has been qualitatively addressed in Ref. 7 by means of photoluminescence (PL) measurements, where an elevated PL intensity by one order of magnitude was seen for passivated CIGS absorbers compared to unpassivated absorbers (i.e. no Al_2O_3 passivation layer) (Joel et al., 2015). Such an improvement in cell performance can be attributed to (i) reduced recombination at the CIGS/Mo–back contact (i.e. effective chemical and field-effect passivation) and (ii) increased carrier collection probability at the space-charge-region due to drift-assisted effective minority carrier diffusion length enhancement. Additionally, Ref (Kotipalli et al., 2015) shows in-depth electrical characterization results on metal–insulator-semiconductor (M-I-S) structures consisting of Al/Al_2O_3/CIGS/Mo, providing a comprehensive picture on the involved, dominant passivation mechanism, and quantifying the surface passivation quality. On the other hand, in van Lare et al. (2015), positive fixed charge dielectric layer grown by ALD-SiO_2 has been successfully integrated into the CIGS, demonstrating improved short-circuit current densities due to strongly enhanced light reflecting rear patterns.

CIGS absorbers have a typical thickness of about 2–3 µm. However, on the way towards mass production, it is necessary to further reduce the thickness. The main reasons are related to material costs, the fact that indium and gallium resources are limited, and because of the need to cut the process duration in order to achieve a higher production throughput (Press release, 2014). However, reducing the CIGS absorber thickness will significantly affect the short-circuit current density (J_{sc}) due to insufficient long wavelength light absorption (van Lare et al., 2015; Press release, 2014). In (Vermang et al., 2014b), it is shown that by introducing a thin layer of Al_2O_3 films in combination with Mo nanoparticles (NPs) as local rear contacts as opposed to the standard Mo-rear contacts can increase the rear internal reflection (R_b) due to angular scattering, thereby improving the absorption of infrared (IR) photons. Such light management techniques are necessary to scatter the photons and provide a second chance in contributing to the electron-hole pair generation, thereby improving the overall J_{sc}. Additionally, the negatively charged Al_2O_3 at the CIGS/Mo interface will induce an E-drift field that will assist the minority carriers towards CdS/CIGS junction, thus improving the overall current collection probability (Vermang et al., 2014, 2014b).

Hence, as a future objective, the ideal approach is to reduce the CIGS absorber layer thickness with the cost advantages of reduced material consumption while maintaining or even boosting the current state-of-the-art lab-scale efficiencies with the following features: (i) reduced bulk recombination (CIGS thickness reduction), (ii) reduced CIGS/Mo rear interface recombination (surface passivation), and (iii) enhanced light confinement (nanostructured rear contacts). Towards that end, to better understand, quantify, and comment on the importance of the above rear passivation concept, there exists a need for simple predictive simulation model that can address the following factors: (i) the influence of chosen rear passivation layer fixed charge type ($+/-Q_f$) and their densities on the solar cell performance, (ii) passivation mechanisms existing at the rear-passivated layer/CIGS interface and their impact on the CIGS thickness variations, (iii) the importance of rear reflection (R_b) while reducing the absorber thickness, (iv) the reasons for discrete gains obtained in the experimental cell efficiencies for different CIGS thicknesses (Vermang et al., 2014, 2013, 2014a, 2014b), and (v) finally, to generalize and propose target "golden parameters" to achieve cell efficiencies > 20% using ultra-thin (0.4–0.5 µm) absorber layers. Therefore, a simplified numerical device model addressing the rear surface passivation effects in CIGS solar cells will allow the TF-PV community to attain a better understanding of the underlying dominant mechanisms on the solar cell performance, to assess experimental (previously reported) cell results, and to further optimize the CIGS solar cell performance. In this paper, we propose and validate a 1-dimensional (D) predictive simulation model to address the rear surface "opto-electronic" effects on CIGS solar cell performances for varying absorber thickness. From the obtained simulation results, we will discuss various device physics concepts that govern the overall cell performances, especially while scaling down the CIGS absorber thickness. Moreover, the proposed simulation model can be generalized to other TF PV technologies (e.g. CZTS, CdTe) that are provided with proper baseline material properties of the respective films.

2. The solar cell device model

All our solar cell structure simulations were performed using 1–Dimension Solar Cell Capacitance Simulator (SCAPS 3.2) thin-film simulation software, under AM 1.5 solar spectrum at 100 mW/cm^2 for J–V characteristics. Cell parameters (namely V_{oc}, J_{sc}, and η) for rear-passivated (RP) and un-passivated (UP) CIGS cells were extracted for varying CIGS thickness and opto-electronic parameters. Next, to realize the rear-passivated CIGS cell structure as well as simultaneously sustain the electrical contacts (between CIGS/Mo) in such 1-D simulation environment, we have introduced an ultra-thin (2 nm) layer (here onward notated as RP-layer), sandwiched in between the actual CIGS absorbing layer and the Mo-back contact. The RP-layer possesses similar baseline properties as the actual CIGS-absorber layer (for contact purpose) with experimentally extracted passivation properties (i.e. Q_f and D_{it}) Kotipalli et al., 2015. Next, implementing fixed charge type ($+/-$) in the RP-layer are achieved by introducing a uniform distribution of single-donor (i.e. for $+Q_f$) or single-acceptor (i.e. for $-Q_f$) in the bulk of the RP-layers respectively. Then the D_{it} insertions into the model are

Table 1
Baseline parameters used for modeling CIGS solar cells.

Parameter	RP-layer	CIGS	OVC	CdS	i-ZnO	ZnO: Al
W (nm)	2	Variable	30	50	200	400
E_g (eV)	1.15	1.15	1.3	2.4	3.3	3.3
χ (eV)	4.5	4.5	4.5	4.45	4.55	4.55
$\varepsilon/\varepsilon_0$	13.6	13.6	13.6	10	9	9
N_c (cm^{-3})	2.2×10^{18}	2.2×10^{18}	2.2×10^{18}	1.3×10^{18}	3.1×10^{18}	3×10^{18}
N_v (cm^{-3})	1.5×10^{19}	1.5×10^{19}	1.5×10^{18}	9.1×10^{18}	1.8×10^{19}	1.8×10^{19}
V_e (cm/s)	3.9×10^7	3.9×10^7	3.9×10^7	3.1×10^7	2.4×10^7	2.4×10^7
V_h (cm/s)	1.4×10^7	1.4×10^7	1.4×10^7	1.6×10^7	1.3×10^7	1.3×10^7
μ_e (cm^2/Vs)	100	100	10	72	100	100
μ_h (cm^2/Vs)	12.5	12.5	1.25	20	31	3
Doping (cm^{-3})	Solar cell: 5×10^{16} (a) M-I-S: 5×10^{10} (a)	5×10^{16} (a)	1.25×10^{13} (a)	5×10^{17} (d)	1×10^{17} (d)	5×10^{19} (d)
			Interface properties			
		CIGS/OVC			OVC/CdS	
ΔE_c (eV)		*0.0*			*0.05*	
N (cm^{-2})		*10^{11} (N)*			*3×10^{13}(N)*	
σ_e *(cm^2)*		*10^{-15}*			*10^{-15}*	
σ_h *(cm^2)*		*10^{-15}*			*10^{-15}*	
			Bulk defect properties****			
N (cm^{-3})	10^{14} (D)	10^{14} (D)	10^{14}(N)	$5 * 10^{16}$(A)	10^{16} (A)	10^{16} (A)
σ_e(cm^2)	10^{-15}	10^{-15}	10^{-15}	10^{-15}	10^{-15}	10^{-15}
σ_h (cm^2)	10^{-11}	10^{-11}	5×10^{-13}	5×10^{-13}	5×10^{-13}	5×10^{-13}

(a) and (d) denote shallow acceptor and donor defect while (A), (D), and (N) denote deep acceptor, donor, and neutral defects, OVC: Ordered Vacancy Compound.
Nomenclature: ΔE_c: Conduction band offset; E_g: Band gap; $\varepsilon/\varepsilon_0$: Relative permittivity; W: Layer thickness; χ: Affinity; μ_e, μ_h: electron and hole mobility; V_e, V_h: Velocity of electrons and holes; E_g (eV): band gap Energy; N_c, N_v: Effective density of states in conduction and valence bands; σ_e, σ_h: Capture cross-section of electrons and holes.

realized by donor-type Gaussian defect distribution at the CIGS/RP-interface. The recombination rate in defects also depends on the capture cross-section and on the thermal velocity. We have assumed a capture cross section of 10^{-16} cm^{-2} for neutral traps (Hirai et al., 2014). The thickness of the RP-layer has been kept at minimum (2 nm) in order to avoid additional photo-response (since this layer possesses CIGS baseline properties). Furthermore, the Ga-grading in the absorbers (both in the CIGS and RP-layers) are kept uniform to avoid complementary passivation effects. Tunneling at contacts is not implemented in our SCAPS simulation model. Additionally, we have simulated the conventional solar cell structures (i.e. CIGS/Mo interface without any RP-layer) for reference. A rear contact barrier height of 0.27 eV is chosen for solar cell structures between the RP/rear-metal contacts. The absorption coefficient of CIGS is kept constant at 10^5 cm^{-1} in all our simulations. Lastly, we have chosen very high quality of absorber layer with lower deep-bulk defects within the CIGS, in order to clearly discriminate the gains due to chemical and field-effect passivation. Table.1 provides the baseline parameters of each layer used in our simulation model (Vermang et al., 2013; Hirai et al., 2014; Song et al., 2004; Gloeckler, 2005).

3. Results and discussion

In Section 3.1, we validate the proposed simulation model for surface passivation effects (i.e. Q_f and D_{it}) on CIGS absorber layer using a simplified M-I-S structure. Next, using complete solar cell structure model, in Sections 3.2–3.6, we discuss the influence of type $(-/+)$, the magnitude of Q_f, D_{it}, and R_b and their impact on the solar cell performances for varying absorber layer thickness. Finally, in Section 3.7, we discuss the results of optimizing the RP-layer to achieve efficiencies > 20% with ultra-thin CIGS absorber thickness. For the sake of clarity, only results with most significant J-V parameter trends are shown and discussed in the following sections (missing J-V parameter plots are provided in supplementary data file).

3.1. RP-layer implementation and model validation

Prior to the simulation of complete solar cell structures, the proposed simulation model is validated for proper implementation of the RP-layer passivation effects (i.e. Q_f and D_{it}). For this purpose, we have studied the influence of Q_f and D_{it} on the CIGS absorber using a simplified M-I-S capacitor structure (Kotipalli et al., 2013, 2015; Nicollian and Brews, 1982). The M-I-S structure consists of an aluminum front-contact gate with a metal work function of 4.15 eV, insulating dielectric passivation (P)-layer which possesses CIGS baseline properties with a lower acceptor doping concentration, 1 µm thick CIGS absorber, and Mo-back contact with a metal work function of 4.6 eV (Kotipalli et al., 2015). Capacitance-voltage (C-V) characteristics are generated for 10 kHz a.c signal frequency under dark conditions, with varying densities of $-Q_f$ and D_{it} (in the P-layer). Fig. 1 (a) represents the simulated C-V characteristics at 10 kHz for a negative fixed charge insulator on CIGS using M-I-S capacitor with a fixed D_{it} of 1×10^{12} cm^{-2} eV^{-1} (i.e. at the passivation-layer/CIGS interface) and varying $-Q_f$ (i.e. uniform acceptor-type defect distribution in the bulk of RP-layer). It is observed that the flat-band voltage of the C-V curves shift towards positive gate voltages, with increasing acceptor type defect density (i.e. $-Q_f$) in the bulk of the RP-layer, meaning that the negative fixed charges in the SCAPS-layer was effectively implemented (i.e. the field-effect passivation) (Kotipalli et al., 2013, 2015; Nicollian and Brews, 1982). Next, Fig. 1(b) shows the C-V characteristics at 1 kHz for varying interface trap charge densities (D_{it}) with a constant experimentally extracted $Q_f = -8 \times 10^{12}$ cm^{-2}(Kotipalli et al., 2015). This has been accomplished by varying the defect density at the CIGS/RP–interface. From the obtained normalized C-V characteristics, we observed the contribution of interface trap charge capacitance (C_{it}) in the inversion voltage regime (i.e. between -5 V to $+5$ V) with increasing D_{it}, indicating that the SCAPS-model accommodates well the chemical passivation effect (Kotipalli et al., 2013; Nicollian and Brews, 1982). Sufficiently large front and rear surface recombination velocities (SRV) of 10^7 cm/s at the metal contacts were chosen in order to clearly discriminate the impact of $-Q_f$ and $+Q_f$ passivation effects (i.e. not to duplicate the effect of rear surface recombination).

3.2. Influence of $-Q_f$ and CIGS absorber thickness on J-V parameters

Here, we introduce the $-Q_f$ in the bulk of RP-layer using device structures comprising of ZnO:Al/i-ZnO/CdS/CIGS/RP-layer/Mo-back contact. Next, solar cell performances are simulated for a fixed

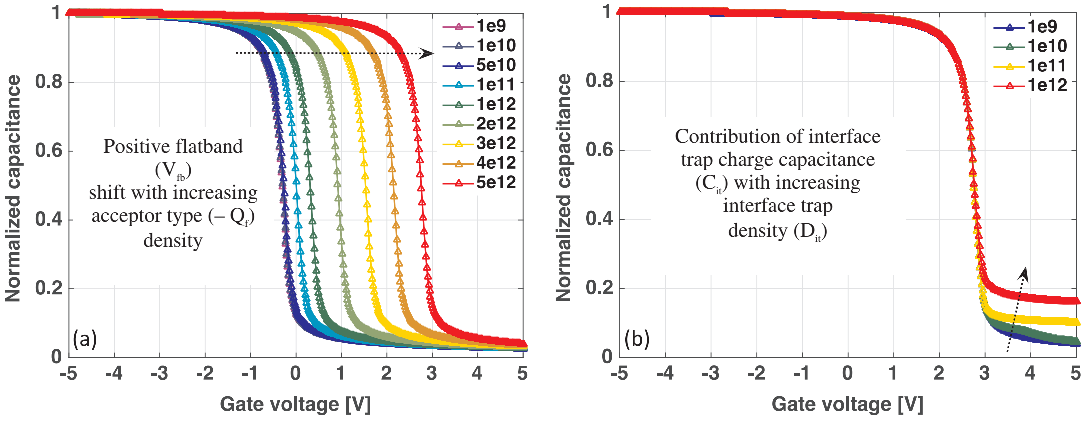

Fig. 1. Simulated Capacitance-Voltage (C-V) characteristics of the M-I-S structure (Al-gate/P-layer/CIGS/Mo). This is performed to validate the passivation effects of the RP-layer on the CIGS absorber layers, by analyzing the following: (a) the influence of field effect passivation due to $-Q_f$ (cm^{-2}) and (b) chemical passivation at the CIGS/RP-interface due to D_{it} ($eV^{-1}\ cm^{-2}$).

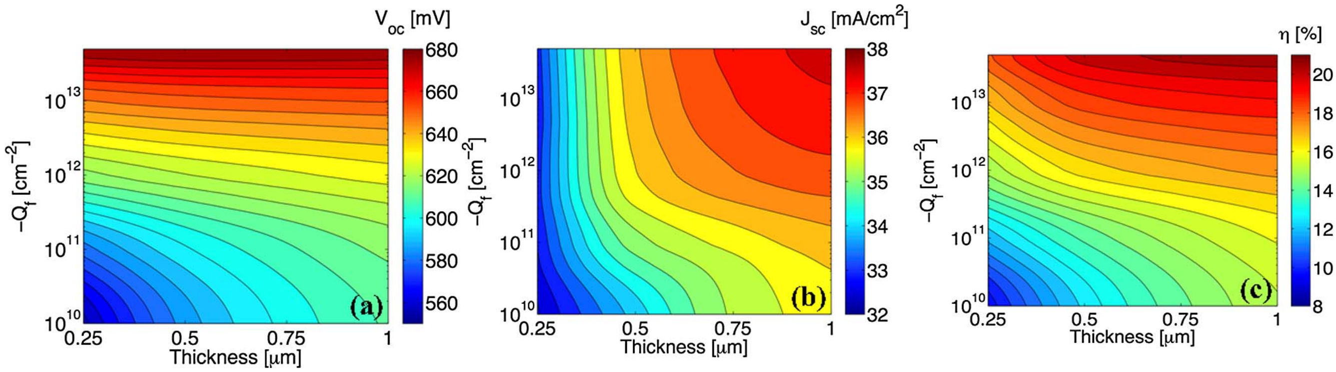

Fig. 2. Simulated J-V parameters of a negatively charged RP CIGS solar cell; (a) open-circuit voltage (b) short-circuit current density, and (c) overall conversion cell efficiency as a function of CIGS absorber thickness, negative fixed charge densities in the RP-layer and with a constant R_b = 70% and R_f = 10%

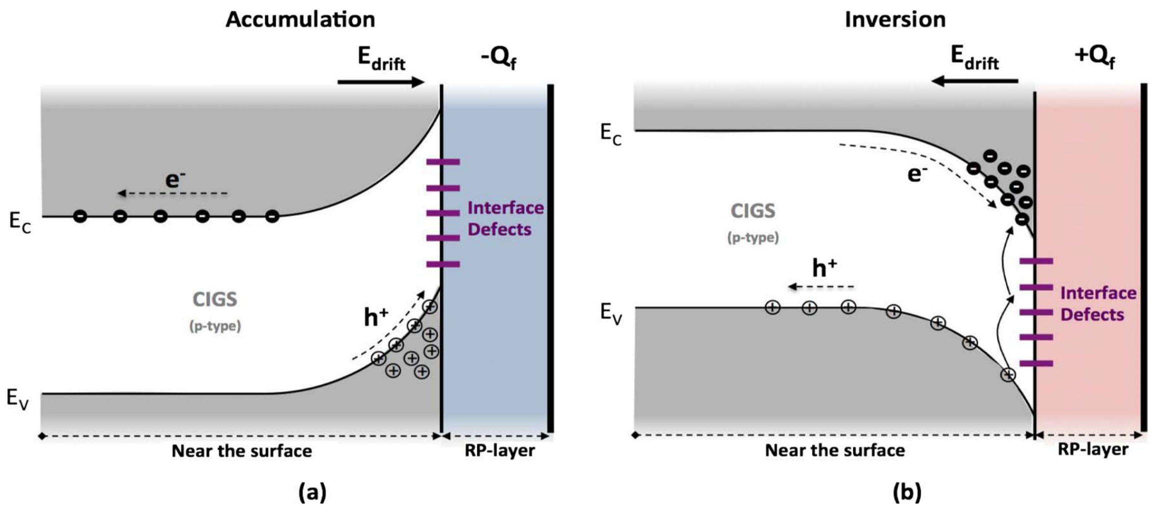

Fig. 3. Energy band bending schematic at the rear CIGS/RP-layer/Mo interface: (a) accumulation condition (field-effect) formed due to $-Q_f$ in the RP-layer, (b) Inversion condition (counter-field effect) formed due to $+Q_f$ in the RP-layer.

$D_{it} = 1 \times 10^{12}\ cm^{-2}\ eV^{-1}$ (i.e. mean values from ref (Kotipalli et al., 2015) as a function of $-Q_f$ and CIGS absorber layer thickness and the resulting V_{oc}, J_{sc} and efficiency plots are shown in Fig. 2(a–c). From these results, for $-Q_f > 5 \times 10^{12}\ cm^{-2}$ we observed improvements in both V_{oc}, J_{sc} and eventually a significant gain in the cell efficiencies especially for thinner regimes (i.e. 0.4–0.6 μm) of the absorber layers, compared against upassivated reference case (presuming $-Q_f = 1 \times 10^{10}\ cm^{-2}$) for similar thickness range. Such gains in cell performance can be explained, thanks to the presence of negative fixed charges in the RP-layer, where the rear surface recombination velocity (S_b) of the CIGS rear surface can be reduced from 1×10^7 cm/s to 1×10^2 cm/s (Hsu et al., 2012). Such a reduction in rear S_b at the CIGS/$-Q_f$: RP-layer/Mo-contact was explained using interface energy band bandings as shown in Fig. 3(a) Dingemans and Kessels, 2012.

The negative fixed charges in the RP-layer shield the minority carriers (here electrons) from being recombined with the interface traps

(Kotipalli et al., 2013, 2015; Hoex et al., 2008; Schmidt et al., 2008; Joel et al., 2015). The negative charges build an internal electric field that repels the minority carriers away from this trap-rich CIGS/Mo-interface (Kotipalli et al., 2013, 2015). The energy band bending shows a pile-up behavior, suggesting a majority carrier accumulation (in this context, holes), and creates an uphill for the conduction band minority carriers from being recombined, thereby reducing the rear S_b (Hoex et al., 2008). Under such low S_b conditions, if the CIGS absorber layer thickness (e.g. < 0.5 μm) becomes less than or comparable to the bulk diffusion length (L_d = 0.5 μm) of the minority carriers, there will be a significant gain in V_{oc} due to considerable enhancement in the effective diffusion length (i.e. due to additional drift field) (Lundberg et al., 2003). Contrarily, for thicker (> 1 μm) CIGS absorber layers, the influence of lower S_b is less significant, thus limiting the gain in V_{oc}. Another advantage in reducing the thickness of the CIGS absorber leads to a reduction in the bulk defects, and thereby an improvement in the overall recombination losses. Next, Fig. 2(b) also shows a significant gain in J_{sc} for lower (~0.5 μm) thickness, which can be explained by the fact that, in thick absorber films, fewer carriers are generated deep into the CIGS absorber layers that have reduced collection probability at the space charge region (SCR). However, for thinner absorber layers, the minority carriers generated beyond the SCR will be drifted towards the SCR thanks to the additional drift electric field (E_{drift}) induced by the high density of $-Q_f$ in the RP-layer. However, on the other hand, reduced quasi-neutral regions (QNR) for extremely thin CIGS absorbers (~0.25 μm) will lead to increased diode-quality factors and thus to reduced FF and efficiencies. Finally, Fig. 2 (c) represents the significant gains in the cell efficiencies, especially for thinner CIGS absorber thickness (< 0.5 μm) due to gains in both V_{oc} (due to reduced rear surface recombination at the CIGS/Mo back contact) in combination with J_{sc} (due to enhanced collection probability at the SCR) (Lundberg et al., 2003).

3.3. Influence of $+Q_f$ and CIGS absorber thickness on J-V parameters

Fig. 4(a,b) present the generated cell parameter results for $+Q_f$ within the RP-layer of the CIGS solar cell. Interestingly, we observed contrary trends in the simulated cell parameters, especially for thinner absorber thickness regimes (0.4–0.6 μm) compared to the $-Q_f$ case. The determinant factors that are influencing the V_{oc} and J_{sc} evolutions can be explained as follows: positive fixed charges in the RP layer will attract minority carriers (here electrons) towards the CIGS/RP-interface and may recombine at the highly recombinative rear contact openings (**Note:** in our simulations a rear metal contact S_b of 10^7 cm/s is considered at the RP/rear-metal contact interface and the RP-layer possesses CIGS-like properties to ensure electrical contact). The minority carrier surface concentration (ns) increases with increasing $+Q_f$ in the RP-layer. For moderate $+Q_f$ (i.e. from 10^{10} to 10^{11} cm^{-2}), moderate densities of electrons are accumulated at the CIGS/RP surface, thereby also a moderate level of recombination occurs at the RP/rear-metal contact. Thus for any given absorber thickness, the decrease in V_{oc} is less pronounced within this range of $+Q_f$ (Kotipalli et al., 2013; Nicollian and Brews, 1982). On the other hand, for higher (> 10^{11} cm^{-2}) $+Q_f$ in the RP-layer an inversion layer (large concentration of electrons) is formed at the CIGS/RP-surface. This conducting inversion layer (n-type) is separated from the p-type CIGS by a depletion layer (Kotipalli et al., 2013). Under such high electron concentrations at the CIGS/RP-surface, the electrons will have free access to the recombination (R) centers (i.e. interface traps) located at the rear-metal contact (Shockley and Read, 1952; Aberle et al., 1992). Moreover, the band bending at the CIGS/RP-layer interface will create a downhill for the electrons to be easily recombined at the rear-interface traps (Kotipalli et al., 2013, 2015; Nicollian and Brews, 1982). Fig. 3(b) shows the energy band bendings for $+Q_f$ charges within the RP-layer. The bands are bent down and the magnitude of band bending depends on the intensity of $+Q_f$ within the RP-layer, thereby surface depletion and/or inversion modes are formed at the CIGS/RP-layer interface. The detrimental effect of high $+Q_f$ in the RP layer can be largely reduced if the rear S_b at the RP/rear-metal contact interface is reduced down to 10^2 cm/s (i.e. reduced R-centers for free electrons). Very high $+Q_f$ (> 5 × $10^{12}$$cm^{-2}$) exhibits strong detrimental effect due to “counter-field effect passivation” mechanism, where the minority carriers (electrons) are accumulated at the CIGS rear surface, thereby creating a parasitic pseudo PN-junction with a built-in potential (V_{bi_rear}), which is placed opposite to the main CdS/CIGS junction (V_{bi_front}), and hence, there is an overall loss in the cells V_{oc} = (V_{bi_front}–V_{bi_rear}).

Next, it is interesting to discuss the impact of high $+Q_f$ (> 5 × 10^{12} cm^{-2}) within the RP-layer and its impact on the CIGS absorber thickness. For this purposes, we have considered two distinct CIGS thickness regimes for discussions;

(i) For ultra-thin CIGS thickness (< 0.4 μm), a downward band bending exists at CIGS/$+Q_f$.RP-layer/Mo interface and this is compensated by an upward band bending at CdS/CIGS interface, thereby a linear downhill band profile being formed within the QNR region with a slope (S_{QNR}). The S_{QNR} within the QNR dictates the counter E_{drift} field-strength pointing towards the CdS/CIGS-front junction and the resulting minority carrier concentration (i.e. increased recombination rate) at the CIGS/Mo-interface with high SRV ~10^7 cm/s (please see Fig. 3b). Therefore, we can describe S_{QNR} as a dependent function of $+Q_f$ (proportional) and CIGS thickness (inversely proportional) and will determine the losses in V_{oc} (i.e. larger S_{QNR} will result in higher V_{oc} losses and vice versa for lower S_{QNR}).

(ii) On the other hand, for CIGS thickness in the range of 0.4–0.6 μm the S_{QNR} is slightly relaxed (i.e. reduced downhill slope) with increasing absorber thickness, thereby an overall improvement in cell efficiencies compared against thinner < 0.4 μm absorber layers. Nevertheless, the front CdS/CIGS junction space charge region (SCR ~ 200–300 nm) being closer to the highly recombinative CIGS/Mo- interface, thereby resulting in noticeable V_{oc} and cell efficiencies losses.

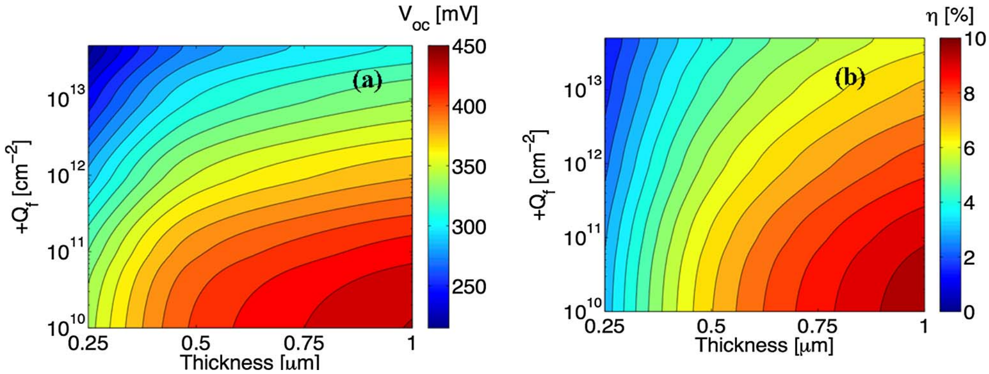

Fig. 4. Simulated J-V parameters of a positively charged rear-passivated CIGS solar cell; (a) open-circuit voltage, and (b) overall conversion cell efficiency as a function of CIGS absorber thickness, positive fixed charge densities within the RP-layer and with a constant R_b = 70% and R_f = 10%.

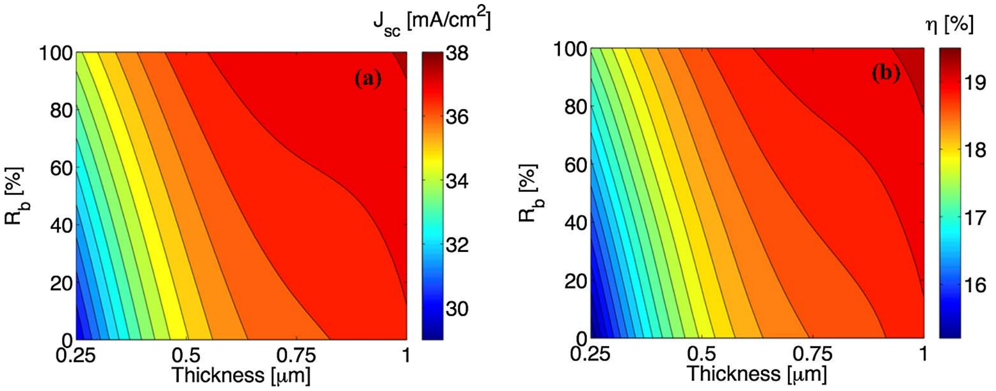

Fig. 5. Simulated (a) short-circuit current density and (b) solar cell efficiency as a function of rear interface reflection and CIGS absorber thickness and for a constant $-Q_f = 8 \times 10^{12}\,cm^{-2}$ within the RP-layer.

3.4. Importance of rear-reflection in ultra-thin CIGS solar cells

Ultra-thin (< 500 nm) CIGS solar cells with no rear-reflection have rather low conversion efficiency due to poor quantum efficiency in the infrared part of the solar spectrum (i.e. a lower absorption of the material in this spectral range). By increasing the light path in the absorber, this drawback can be avoided. These effects can be obtained by introducing excellent rear reflecting structures (van Lare et al., 2015; Andreani et al., 2012; Trompoukis et al., 2015; Poncelet et al., 2017). Therefore, a major part of the light that is not absorbed into the CIGS layer during the first passage is reflected back into the absorber during the second time (and possibly during the following times), increasing significantly the probability for photons to be absorbed (light path enhancement). Consequently, the energy conversion efficiency of the device improves due to enhancement in the J_{sc}. Hence, in this section, we will analyze the impact of rear reflection on the CIGS absorber thickness for a reduced rear interface recombination by implementing $-Q_f$ passivation effects in the RP-layer. From Fig. 5(a), for CIGS absorber thickness (W) of 0.25 µm, very low J_{sc} values are obtained, and these effects can be explained using the following involved mechanisms: (i) the optical loss related to insufficient absorption capacity of the CIGS absorber layer, (ii) recombination at the front CdS/CIGS interface (Note: we have optimized the rear interface recombination velocity $S_b < 100\,cm/s$ by introducing $-Q_f$ in the RP-layer), and (iii) recombination in the space charge region (SCR). An SCR width (d) in the range of 0.2–0.25 µm was generally reported in literature for ungraded CIGS absorbers, and it has a significant effect on the carrier collection, especially while scaling the CIGS absorber thickness closer to the SCR widths (d = W). In principle, the electric field within the SCR ensures efficient collection of photo-generated carriers in the SCR as well as the charge reaching the SCR by the diffusion component from the neutral part (i.e. outside the SCR) of the CIGS (Kosyachenko, 2013). Thinning the CIGS layer reduces the current density J_{sc}, primarily, because of the removal of the photocurrent diffusion component (i.e. loss of photocurrent contribution outside the SCR). However, improvements in J_{sc} (Fig. 5a) and cell efficiencies (Fig. 5b) are expected to increase (even for $R_b \sim 70\%$) by choosing slightly thicker CIGS absorber (i.e. W > d). For CIGS absorber thickness in the range of 0.4–0.6 µm, we see a noticeable gain in the J_{sc} due to additional neutral-region photocurrent diffusion component and improved rear S_b and R_b components. Indeed, ref's (Vermang et al., 2014, 2014a, 2014b) showed improved long-wavelength EQE response and Jsc gains of 3.4 mA/cm^2 due to improved rear photon scattering effects compared to a standard back contact ($R_b < 50\%$) for ultra-thin 380 nm CIGS thickness. These results agree very well with our simulation model trends as shown in Fig. 5(a). Finally, the influence of rear R_b becomes less significant for thick absorbers (i.e. beyond 0.8 µm), since most of the light will be absorbed by the CIGS layer (Kosyachenko, 2013).

3.5. Impact of chemical passivation (D_{it}) under strong field-effect passivation

From Section 3.3, it is clear that $+Q_f$ charges within the RP-layer were found to be detrimental to the solar cell performance, especially for ultra-thin CIGS absorber layers. Hence, to better understand the influence of rear interface trap density effects on the cell performance, in this section, we have considered $-Q_f$ within the RP-layer. A typical value of $-Q_f$ within the RP-layer was taken from previously reported experimental values and kept constant at 8×10^{12} cm^{-2}, while the D_{it} and CIGS absorber thickness are varied during the simulations (Kotipalli et al., 2015). Fig. 6 (a,b) shows the resulting V_{oc} and the corresponding efficiency plots. From these results, we clearly observe that the influence of D_{it} is almost independent of absorber thickness for interface trap densities $< 5 \times 10^{12}\,eV^{-1}\,cm^{-2}$. However, a noticeable impact on V_{oc} and cell efficiencies is observed for $D_{it} > 5 \times 10^{12}\,eV^{-1}\,cm^{-2}$ and these effects are predominant only for ultra-thin regimes (< 0.4 µm) of absorber layers compared to the thicker ones. This phenomenon can once again be explained due to the front SCR (of the CdS/CIGS junction) being closer to the highly recombinative rear trap-rich interface (Poncelet et al., 2017). Although,

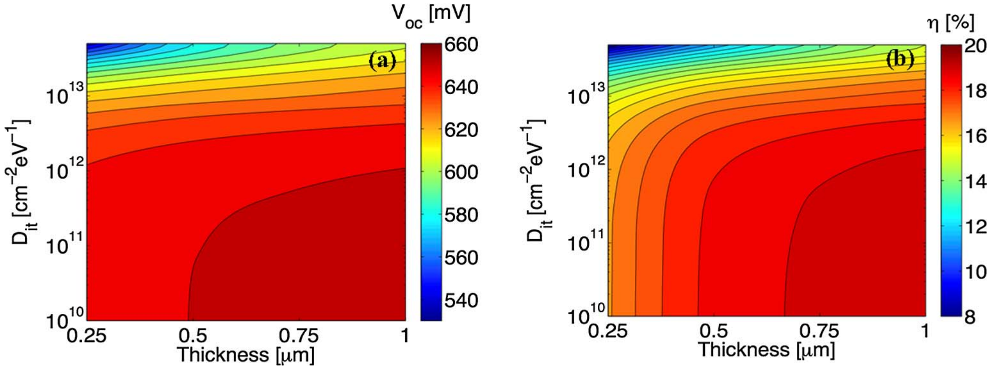

Fig. 6. Simulated CIGS solar cell parameters; (a) open-circuit voltage and (b) cell efficiency as a function of rear interface trap densities and CIGS absorber thickness, with a constant fixed negative charge of $8 \times 10^{12}\,cm^{-2}$ within the RP-layer for a constant $R_b = 70\%$ and $R_f = 10\%$.

$-Q_f$ in the RP-layer may compensate for the recombination process to some extent: thanks to the built-in electric field, the net concentration of minority carriers (n_s) at the CIGS surface will be reduced, thereby satisfying one of the requirements to reduce the surface recombination velocity (S_b), according to the Shockley–Read–Hall formalism (Shockley and Read, 1952; Aberle et al., 1992; Poncelet et al., 2017). However, another major requirement to lower the S_b is to reduce the rear D_{it} at the CIGS/RP-layer interface for an optimal cell performance. Hence, the effective S_b at the rear CIGS/RP-interface can be considered as a trade-off between the field-induced passivation (due to $-Q_f$) and interface chemical passivation (due to D_{it}). However, when the magnitude of D_{it} becomes sufficiently larger ($> 5 \times 10^{12}\,eV^{-1}\,cm^{-3}$), we observe the S_b reduction due to the field-effect passivation gets less significant, and eventually starts affecting the solar cell performance (mainly a loss in the V_{oc}) due to increased interface trap recombination. In ref (Kotipalli et al., 2015), we have shown experimentally extracted D_{it} values of $(8.1–15.0) \times 10^{11}\,eV^{-1}\,cm^{-2}$ for negatively charged Al_2O-layer with a $-Q_f$ value of $8 \times 10^{12}\,cm^{-2}$. The resulting V_{oc} for uniformly graded 0.4 µm –thick CIGS solar cells demonstrated Voc's in range 633–649 mV, which agrees well with the V_{oc} trends obtained using our simulation model for the similar value of $-Q_f$ and D_{it} within the RP-layer (see Fig. 6a).

3.6. Influence of chemical passivation without strong field-effect passivation

In Section 3.5, we have discussed the impact of chemical passivation (D_{it}) under strong field-effect ($-Q_f \sim 8 \times 10^{12}\,cm^{-2}$) conditions. However, it is worth to study the impact of chemical passivation solely on the absorber thickness and resulting J-V parameters. To achieve this, we have reduced the $-Q_f$ density from $8 \times 10^{12}\,cm^{-2}$ to $1 \times 10^{8}\,cm^{-2}$ (i.e. almost no field-effect passivation), where the D_{it} densities were varied from 1×10^{10} to $1 \times 10^{13}\,eV^{-1}\,cm^{-2}$ for a constant $R_b = 70\%$ and $R_f = 10\%$. From Fig. 7 (a,b) we can clearly observe that for a given absorber thickness, the impact of chemical passivation is almost independent on the D_{it} level. However, for extremely thin absorber regimes (0.25–0.4 µm) there exists a small loss in V_{oc} and cell efficiencies for thinner absorber layers compared to thicker ones, especially for $D_{it} > 5 \times 10^{12}\,eV^{-1}\,cm^{-2}$. By comparing Fig. 7 (a,b) and Fig. 6 (a,b), conclusion can be drawn that for $D_{it} < 5 \times 10^{12}\,eV^{-1}\,cm^{-2}$ field-effect passivation dominates the chemical passivation for wide range of absorber thickness. However, for extremely larger $D_{it} > 5 \times 10^{12}\,eV^{-1}\,cm^{-2}$ very small effect on the cell performance losses can be seen.

3.7. Influence of field-effect passivation without chemical passivation

In this section we will see the impact of field-effect passivation strength versus the absorber thickness excluding the detrimental effects of traps at the CIGS/RP-interface. To realize this model, we have fixed the D_{it} to $1 \times 10^{8}\,eV^{-1}\,cm^{-2}$ (i.e. an excellent chemical passivation), where the $-Q_f$ density in the RP-layer is varied from 1×10^{10} to $1 \times 10^{13}\,cm^{-2}$ for constant $R_b = 70\%$ and $R_f = 10\%$. Unlike the previous sections, where we have discussed in detail the significance of $-Q_f$ on V_{oc} and J_{sc} parameters for varying absorber thickness and the underlying physics, in this section, we will focus on the net gains in cell efficiencies for different field-effect passivation strengths (i.e. $-Q_f$ densities) versus CIGS thickness. Fig. 8 shows the obtained gains in cell efficiency solely due to field-effect passivation without any negative effects of interface traps (D_{it}). From these results, it is clear that $-Q_f > 5 \times 10^{12}\,cm^{-2}$ is required in order to achieve reasonable cell efficiencies especially for ultra-thin (0.4–0.6 µm) CIGS absorbers. These results also demonstrate the fact that field-effect passivation gets less pronounced with increasing absorber thickness. Next, less noticeable gains in cell efficiencies were observed for $-Q_f$ below $1 \times 10^{12}\,cm^{-2}$ and it even gets worse ($< 1\%$ gain) for thicker (> 0.75 µm) absorber layers.

3.8. Experiments versus proposed model

In Sections 3.2,3.4, and 3.5 we have discussed general trends in CIGS solar cell parameters and the involved mechanisms related to the rear passivation. In this section, we will focus our discussions on the discrete gains (*absolute*) in V_{oc}, J_{sc}, and η using our simulation model in order to highlight the significance of each of the optoelectronic properties or a combination of these properties that governs the various device mechanisms. Table.2 provides the extracted (experimental) cell parameters for both unpassivated and rear passivated devices for different absorber thicknesses. Identical quality of CIGS films (see Table.1) was used for all the thickness cases with uniform gallium grading profiles in the simulation model similar to the experimental case. Next, the negatively charged Al_2O_3 RP-layers used in the experiments are mimicked in our simulation model by considering negative fixed charge density of $8 \times 10^{12}\,cm^{-2}$ and interface charge density of $1 \times 10^{12}\,eV^{-1}\,cm^{-2}$ as the RP-layer properties. The reported results in Table 2 are separated into two different Groups A (thinner) and B (thicker) comprising of 0.24–0.4 µm cases and 1.1–1.5 µm cases respectively. From the same Table 2, we can observe a strong dependency in the cell parameters on the absorber layer thickness (i.e. thinner absorber films exhibit significant improvement in both V_{oc} and J_{sc} compared to thicker films). Group A samples underwent front surface MgF_2 anti-reflective coatings (ARC), while no such ARC films were deposited in the fabrication of Group B samples. This effect in front surface reflection for Group A samples was included by adjusting the front reflection (R_f) parameter in the device simulator. Hence, R_f and R_b of 5% and 70%

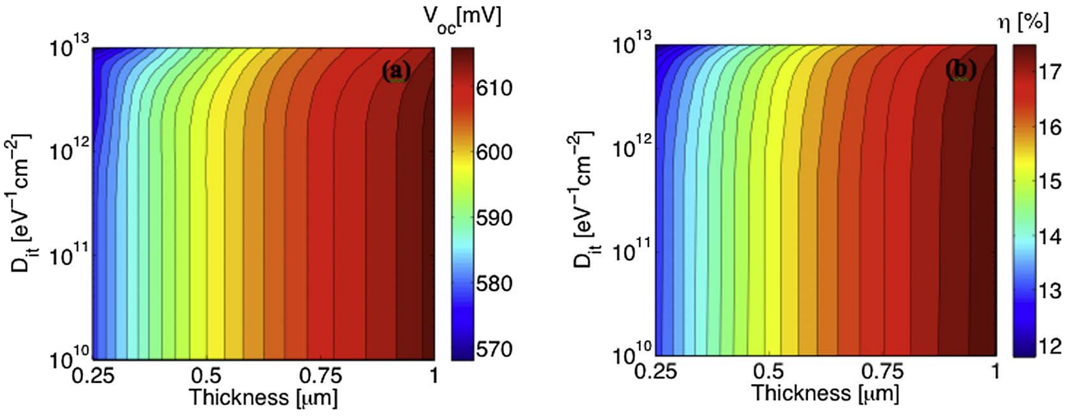

Fig. 7. Simulated CIGS solar cell parameters; (a) open-circuit voltage and (b) cell efficiency as a function of rear interface trap densities and CIGS absorber thickness, with a constant fixed negative charge of $1 \times 10^{8}\,cm^{-2}$ within the RP-layer for a constant $R_b = 70\%$ and $R_f = 10\%$.

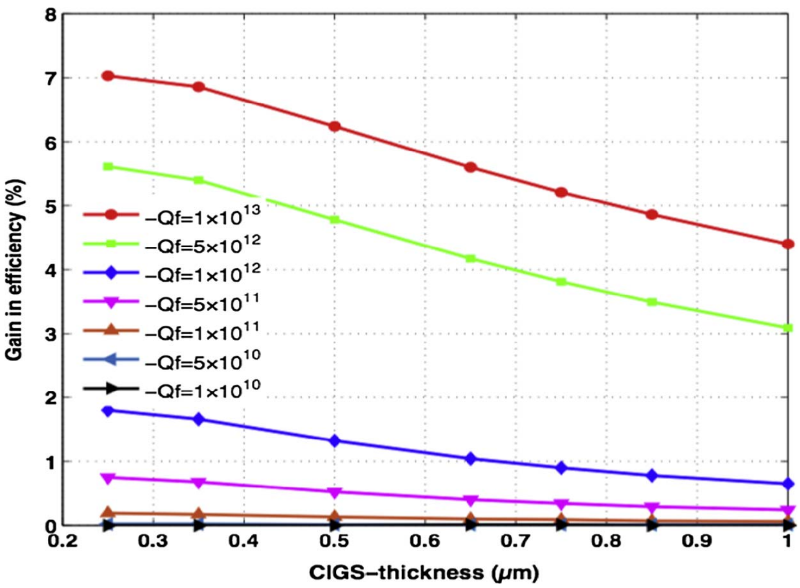

Fig. 8. Absolute gain in cell efficiencies [estimated from the difference between; case (i) varying field-effect passivation (i.e. $-Q_f$ from $1 \times 10^{10}\,cm^{-2}$ to $1 \times 10^{13}\,cm^{-2}$) and with constant, excellent chemical passivation ($D_{it} = 1 \times 10^8 eV^{-1}\,cm^{-2}$) and case (ii) excellent chemical passivation ($D_{it} = 1 \times 10^8 eV^{-1}\,cm^{-2}$) with no field-effect passivation ($-Q_f = 1 \times 10^8\,cm^{-2}$)] solely due to field-effect passivation strengths as a function of CIGS thickness for constant $D_{it} = 1 \times 10^8 eV^{-1}\,cm^{-2}$, $R_f = 10\%$ and $R_b = 70\%$

respectively were chosen for Group A sample simulations versus 10% and 30% for Group B samples. Additionally, it is also important to note that Group B samples undergo industrial contacting schemes (i.e. spherical shaped nano-sphere precipitates dip in chemical bath solution), yielding uncontrollable (i.e. density, spacing and non-uniform distribution) rear metallization fraction. Thereby resulting in best and worst contacting schemes for 0.4 μm thickness (samples from Group A) and 1.1 μm thickness (samples from Group B) respectively. Moreover, unpassivated reference cells from 1.1 μm samples demonstrated low performances and can be considered as poor cells, which makes these data points invalid for comparison against the modeled efficiencies.

For a fixed rear RP layer negative fixed charge densities ($-Q_f$) and interface trap density (D_{it}):

(i) A strong decrease in V_{oc} gains was observed while increasing the absorber thickness (i.e. from 0.24 to 1.5 μm). This means that the effect of bulk recombination (at the CIGS grain volume) increases as a function of absorber thickness, thereby counter-affecting the gains due to field-effect passivation, leading to noticeable loss in the Voc's (especially from group A to B).

(ii) Next, the gain in J_{sc} gradually reduces and even becomes negative from thinner to thicker absorber layers (i.e. from group A to B). Noticeable gains in Group A samples can be due to several possible mechanisms, such as: (a) effective front R_f (i.e. due to ARC) and rear R_b (i.e. due to MgF_2/Al_2O_3 rear stack) optical confinements, (b) drift-field assisted minority carrier diffusion length enhancement, (c) additional photo-current diffusion component outside the SCR (i.e. quasi-neutral region), (d) diffusion length (L_d) of the minority carriers sufficiently larger than the thickness (0.5 μm) of the absorber layer (ex: $L_d > 0.5$ μm), where the significance of all these effects will be reduced with increasing absorber thickness. On the other hand, a negative gain in J_{sc} (for group B samples) can be attributed to the loss in fill factor (FF) due to improper rear contact formation through the Al_2O_3 passivation layer (resulting in contact resistance losses). The rear contact openings were implemented in an industrial proof-of-concept schemes (i.e. by using nano-sphere shaped precipitates in chemical bath deposition dip) resulting in uncontrolled density of rear-contact openings, and their resulting rear contact metallization fraction, thereby affecting series resistance and FF. These effects were not considered in our simulation model due to 2-D device geometrical mesh requirements.

(iii) Lastly, significant gain in cell efficiencies are seen for thinner absorber films (Group A samples) due to reduced rear surface recombination in combination with improved collection probability at the SCR. These gains in cell efficiencies are limited for thicker films (Group B samples) due to losses in both J_{sc} and FF.

Fig. 9 represents the comparison of predicted efficiencies using our model versus the experimentally obtained cell efficiencies. From the comparison plot, we can clearly see that the simulation model yields higher efficiencies than the experimental results for both passivated and unpassivated cases for all the thickness considered. Such disagreement can be explained due; (i) absorption profile (over the entire wavelength range) mismatch between the SCAPS model and experimental CIGS films, (ii) impact of both series and shunt resistance on the FF, and (iii) uniform R_b and R_f profiles over entire wavelength range (in our SCAPS model), where as in practice (experimentally) this is not the case. Next, it is worth mentioning that the absorption coefficient ($10^5\,cm^{-1}$) in our SCAPS model is kept constant over the entire wavelength range, while in practice this is not being the case. This optical factor plays an important role especially for thinner absorber layers, therefore the current density of thinner CIGS layers is slightly over estimated.

Table 2
Average values and absolute gains in the V_{oc}, J_{sc}, and η of un-passivated reference cells (Ref. cell) and Al_2O_3 passivated cells (pass. cell) for different CIGS absorber thicknesses.

Group	$w_{\_CIGS}$ (μm)	# cells	Average V_{oc} (mV)			Average J_{sc} (mA/cm^2)			Average η (%)		
			Ref. cell	Pass. cell	Abs. gain	refcell	pass cell	abs (gain)	ref cell	pass cell	abs (gain)
A	0.24 Vermang et al., 2014a	4	602	659	57	19.6	23.3	3.7	8.0	11.8	3.8
	0.40 Vermang et al., 2014	6	576	644	68	23.2	30.2	7	9.1	13.2	4.1
B	1.10 Vermang et al., 2014	10	608	645	37	29.4	29.0	–0.4	13.0	13.1	0.1
	1.5 Vermang et al., 2013	8	624	640	16	30.5	30.0	–0.5	14.9	15.1	0.2

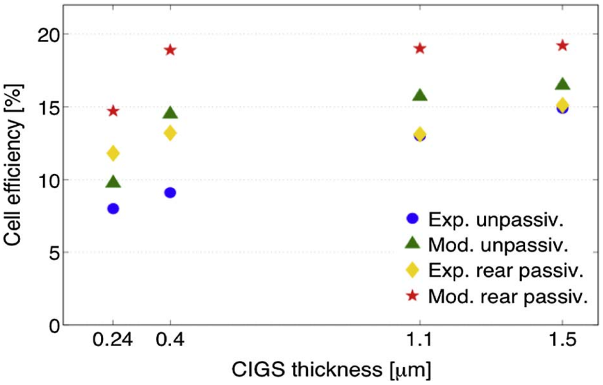

Fig. 9. Experimental (exp.) and simulated (mod.) cell efficiencies for unpassivated and passivated CIGS solar cells versus absorber layer thickness. For front and rear reflectance in the simulation model, we have considered; $R_f = 5\%$, $R_b = 70\%$ for Group A samples and $R_f = 10\%$, $R_b = 30\%$ for Group B samples respectively.

3.9. Rear passivation layer (RP-layer) optimization

In this section, we summarize the requirement for optimal opto-electronic properties of the RP-layer in order to achieve cell efficiencies > 20%, while simultaneously maintaining ultra-thin (0.4–0.6 μm) absorber thickness. Fig. 10 shows the simulated cell efficiencies for the following three different cases: (i) negative (red), (ii) positive (blue) fixed charge densities of $8 \times 10^{12}\ \mathrm{cm}^{-2}$ in the RP-layer, and (iii) without (green) any rear RP-layer (i.e. unpassivated) for fixed $D_{it} = 1 \times 10^{12}\ \mathrm{eV}^{-1}\ \mathrm{cm}^{-2}$, $R_b = 95\%$ and $R_f = 0\%$ as a function of CIGS absorber thickness. From these results, it is clear that the CIGS absorber thickness in the range 0.4–0.6 μm are sufficient to achieve cell efficiencies > 20%, while choosing negative fixed charged RP-layer. We also observe significant gain, especially in the cells V_{oc} and J_{sc} for thinner absorber layers due to (i) reduced rear surface recombination by shielding the minority carriers (i.e. accumulation-mode) and (ii) creating additional electric field (drift component) that assists the minority carriers towards the SCR. On the other hand, cell structures with $+Q_f$ show detrimental effects on the cell performance due to surface depletion (for moderate $+Q_f$) and/or inversion modes (of high $+Q_f$), where one can expect maximum recombination or a parasitic pseudo PN-junction, hindering the open-circuit voltage, and thereby, the cell performance. Finally, cell structures with no RP-layers demonstrate moderate efficiencies amongst the best $(-Q_f)$ and worst $(+Q_f)$ cell performances. One of the limitation factor for the performance of un-passivated CIGS solar cell is the high rear surface recombination velocities ($S_b \sim 10^7$ cm/s) due to large densities of interface traps at the metal (Mo)-Semiconductor (CIGS) interface, where a noticeable loss in both V_{oc} and J_{sc} can be observed for ultra-thin CIGS thickness (< 0.4 μm). Lastly, by comparing the results from Fig. 9 (red[1] stars) and Fig. 10 (red stars) we clearly observe the gains due to both front and rear optical confinement effects.

To summarize, Fig. 11 showcases the impact of five different combinations (#1–5) of passivation mechanisms, with or without optical optimizations on four different absorber layers. From the same figure, we can clearly see the impact of worst (case1) and best (case 2) chemical passivation on ultra-thin (< 0.5 μm) absorber layers. Cases 4 and 3 respectively provide experimental passivation scenarios, with or without optical optimizations resp., as a future roadmap towards > 20% even for thickness ~0.5 μm. Finally, case 5 dominates the efficiency chart amongst all the cases considered, with excellent field-effect and chemical passivation even without the need for further optical optimizations.

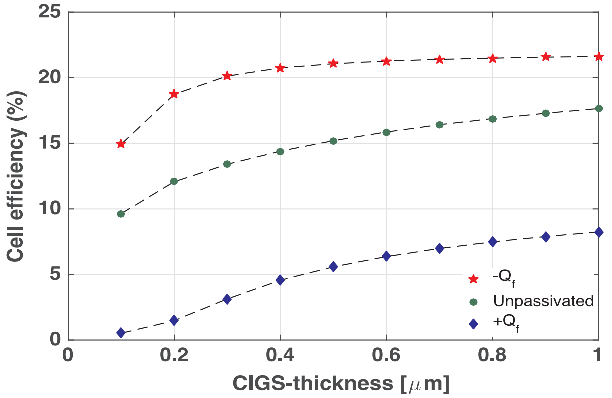

Fig. 10. Simulated CIGS cell efficiencies for varying absorber thickness with fixed (i) $-Q_f = 8 \times 10^{12}\ \mathrm{cm}^{-2}$ (ii) $+Q_f = 8 \times 10^{12}\ \mathrm{cm}^{-2}$ with constant $D_{it} = 1 \times 10^{12}\ \mathrm{cm}^{-2}\ \mathrm{eV}^{-1}$, $R_b = 95\%$ and $R_f = 0\%$.

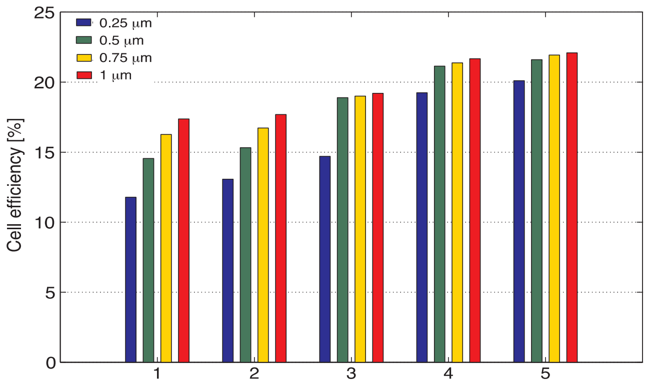

Fig. 11. Overview of different passivation scenarios and their combinations with and without optical optimizations for four different CIGS absorber thicknesses.

4. Conclusions

To improve the understanding of rear surface passivated CIGS solar cells, a predictive simulation model is developed in SCAPS. The implementation of rear passivation layer into the simulation model has been validated using Mo/CIGS/RP-layer/Al M-I-S structures with experimentally reported Q_f and D_{it} values. Next, the proposed model is validated against experimental cell results for different absorber layer thicknesses. From these results, the requirements and limitations on the type (+/–) of fixed charges, their densities, and interface trap densities for enhanced cell performance are established. It is observed that the influence of field effect passivation due to negative fixed charges in the RP-layer is more predominant for thinner absorber layers than for thicker ones, which agrees well with the experimentally reported results. Additionally, we provide the minimum density of $-Q_f$ required and maximum acceptable limit for D_{it} is around $5 \times 10^{12}\ \mathrm{cm}^{-2}$ and $1 \times 10^{13}\ \mathrm{cm}^{-2}\ \mathrm{eV}^{-1}$ respectively. Next, the impact of rear optical reflection R_b can be seen for CIGS thickness greater than the SCR widths. Furthermore, to conclude, it is observed that for Al_2O_3 passivated CIGS surfaces, the field-effect passivation (due to $-Q_f$) is more predominant than the chemical passivation (due to D_{it}). Lastly, we provided guidelines to achieve cell efficiencies > 20% for ultra-thin absorber layers with due consideration of optical (R_b and R_f) and electronic (field-effect and chemical passivation) properties.

5. Outlook

The proposed simulation model and results could be used as a starting point to create complex 2 D models of 3 D cell geometries. These complex device simulators are required in order to find an

---

[1] For interpretation of color in Fig. 9, the reader is referred to the web version of this article.

optimal tradeoff between reduced rear surface recombination losses and rear-metal contact series resistance losses. These rear contact designs should be tested against large variety of optical, electronic and physical properties (ex: thickness of CIGS, doping concentration, minority carrier diffusion lengths, rear contact resistance, rear contact barrier potentials, rear contact SRV, front and rear optical confinement effects, etc…) in order to understand the impact of each parameter and their optimization. Furthermore, such device models will also facilitate the TF-PV research community to implement novel ultra-thin CIGS cell structures with high efficiency capabilities.

Acknowledgements

We gratefully acknowledge to Dr. Marc Burgelman, University of Gent, Belgium, for providing the SCAPS simulation software. This project has received funding from the European Union’s Horizon 2020 research and innovation program under grant agreement No. 720887, and from the European Research Council (ERC) under the European Union's Horizon 2020 research and innovation programme (grant agreement No. 715027). Additionally, B. Vermang acknowledges the financial support of the Flemish Research Foundation FWO (mandate 12O4215N). Finally, R. Kotipalli acknowledges the financial support of a UCL FSR grant.

Appendix A. Supplementary material

Supplementary data associated with this article can be found, in the online version, at http://dx.doi.org/10.1016/j.solener.2017.08.055.

References

Aberle, A.G., Glunz, S., Warta, W., 1992. Impact of illumination level and oxide parameters on Shockley–Read–Hall recombination at the Si-SiO_2 interface. J. Appl. Phys. 71, 4422. http://dx.doi.org/10.1063/1.350782.

Andreani, L.C., Kowalczewski, P.A., Mura, C.I., Patrini, M., Acciarri, M., Binetti, S., Sassella, A., Marchionna, S., 2012. Towards CIGS slar cells with reduced film thickness: a study of optical properties and of photonic structures for light trapping. In: 27th European Photovoltaic Solar Energy Conference and Exhibition, pp. 2334.

Blakers, A.W., Wang, A., Milne, A.M., Zhao, J., Green, M.A., 1989. 22.8% efficient solar cell. Appl. Phys. Lett. 55, 1363–1365.

Chirilă, A., Reinhard, P., Pianezzi, F., Bloesch, P., Uhl, A.R., Fella, C., Kranz, L., Keller, D., Gretener, C., Hagendorfer, H., Jaeger, D., Erni, R., Nishiwaki, S., Buecheler, S., Tiwari, A.N., 2013. Potassium-induced surface modification of Cu(In, Ga)Se2 thin films for high-efficiency solar cells. Nat. Mater 12 (12), 1107–1111.

Deng, W., Chen, D., Xiong, Z., Verlinden, P.J., Dong, J.W., Ye, F., Li, H., Zhu, H.J., Zhong, M., Yang, Y., F Chen, Y., Feng, Z.Q., Altermatt, P., 2015. 20.8% PERC Solar Cell on 156 mm × 156 mm P-Type Multicrystalline Silicon Substrate. IEEE J. Photovolt. 6 (1) 10.1109/JPHOTOV.2015.2489881.

Dhere, N.G., 2007. Toward GW/year of CIGS production within the next decade. Sol. Energy Mater. Sol. Cells 91, 1376–1382. http://dx.doi.org/10.1016/j.solmat.2007.04.003.

Dingemans, G., Kessels, W.M.M., 2012. Status and prospects of Al_2O_3-based surface passivation schemes for silicon solar cells. J. Vac. Sci. Technol. A 30, 040802. http://dx.doi.org/10.1116/1.4728205.

Dullweber, T., Rau, U., Contreras, M.A., Noufi, R., Schock, H.W., 2000. Photogeneration and carrier recombination in graded gap Cu(In, Ga)Se2 solar cells. IEEE Trans. Electron Devices 47 (12), 2249–2254 10. 1109/16.887004.

Dullweber, T., Lundberg, O., Malmstrm, J., Bodegrd, M., Stolt, L., Rau, U., Schock, H.-W., Werner, J.H., 2001. Back surface band gap gradings in Cu(In, Ga)Se2 solar cells. Thin Solid Films 387 (1–2), 11–13. http://dx.doi.org/10.1016/ s0040- 6090(00)01726- 0.

Dullweber, T., Hanna, G., Rau, U., Schock, H.W., 2001. A new approach to high-efficiency solar cells by band gap grading in Cu(In, Ga)Se2 chalcopyrite semiconductors. Sol. Energy Mater. Sol. Cells 67 (1–4), 145–150.

Edoff, M., Schleussner, S., Wallin, E., Lundberg, O., 2011. Technological and economical aspects on the influence of reduced Cu(In, Ga)Se2 thickness and Ga grading for co-evaporated Cu(In, Ga)Se2 modules. Thin Solid Films 519 (21), 7530–7533. http://dx.doi.org/10.1016/j.tsf.2011.01.369.

Gabor, A.M., Tuttle, J.R., Bode, M.H., Franz, A., Tennant, A.L., Contreras, M.A., Noufi, R., Jensen, D.G., Hermann, A.M., 1996. Band-gap engineering in Cu(In, Ga)Se2 thin films grown from (In, Ga)2Se3 precursors. Sol. Energy Mater. Sol. Cells 41–42, 247–260. http://dx.doi.org/10.1016/0927- 0248(95)00122- 0.

Gloeckler, M., 2005. Device Physics of Cu(In, Ga)Se_2 Thin-Film Solar Cells. Ph.D. Thesis. Colorado State University, Fort Collins.

Gloeckler, M., Sites, J.R., 2005. Band-gap grading in Cu(In, Ga)Se2 solar cells. J. Phys. Chem. Solids 66 (11), 1891–1894. http://dx.doi.org/10.1016/j. jpcs.2005.09.087.

Green, M.A., 2015. The passivated emitter and rear cell (PERC): from conception to mass production. Sol. Energy Mater. Sol. Cells 143, 190–197.

Hirai, Y., Kurokawa, Y., Yamada, A., 2014. Numerical study of Cu(In, Ga)Se2 solar cell performance toward 23% conversion efficiency. Jpn. J. Appl. Phys. 53 (1), 012301.

Hoex, B., Schmidt, J., Pohl, P., van de Sanden, M.C.M., Kessels, W.M.M., 2008. Silicon surface passivation by atomic-layer-deposited Al_2O_3. J. Appl. Phys. 104 044903-1-044903-12.

Hsu, W.W., Chen, J.Y., Cheng, T.H., Lu, S.C., Ho, W.S., Chen, Y.Y., Chien, Y.J., Liu, C.W., 2012. Surface passivation of Cu(In, Ga)Se2 using atomic layer deposited Al_2O_3. Appl. Phys. Lett. 100, 023508. http://dx.doi.org/10.1063/1.3675849.

Jackson, P., Hariskos, D., Wuerz, R., Wischmann, W., Powalla, M., 2014. Compositional investigation of potassium doped Cu(In,Ga)Se2 solar cells with efficiencies up to 20.8%. Phys. Status Solidi Rapid Res. Lett. 8 (3), 219–222.

Jackson, P., Wuerz, R., Hariskos, D., Lotter, E., Witte, W., Powalla, M., 2016. Effects of heavy alkali elements in Cu(In, Ga)Se2 solar cells with efficiencies up to 22.6%. Phys. Status Solidi RRL 1–4. http://dx.doi.org/10.1002/pssr.201600199.

Joel, J., Vermang, B., Larsen, J., Donze-Gargand, O., Edoff, M., 2015. On the assessment of CIGS surface passivation by photoluminescence. Phys. Status Solidi RRL 9 (5), 288–292. http://dx.doi.org/10.1002/pssr.201510081.

Kaelin, M., Rudmann, D., Tiwari, A.N., 2004. Low cost processing of CIGS thin film solar cells. Sol. Energy 77 (6), 749–756.

Kosyachenko, L.A., 2013. Possibilities to decrease the absorber thickness reducing optical and recombination losses in CdS/CdTe solar cells. Mater. Renew. Sust. Energy. 3 (2), 1–20.

Kotipalli, R., Delamare, R., Poncelet, O., Tang, X., Francis, L.A., Flandre, D., 2013. Passivation effects of atomic-layer-deposited aluminum oxide. EPJ Photovolt. 4. http://dx.doi.org/10.1051/epjpv/2013023.

Kotipalli, R., Vermang, B., Fjällström, V., Edoff, M., Delamare, R., Flandre, D., 2015. Influence of Ga/(Ga + In) grading on deep-defect states of Cu(In, Ga)Se2 solar cells. Phys. Status Solidi RRL 9, 157–160. http://dx.doi.org/10.1002/pssr.201510024.

Kotipalli, R., Vermang, B., Joel, J., Rajkumar, R., Edoff, M., Flandre, D., 2015. Investigating the electronic properties of Al2O3/Cu(In, Ga)Se2 interface. AIP Adv. 5, 10710. http://dx.doi.org/10.1063/1.4932512.

Lundberg, O., Bodegard, M., Malmstrom, J., Stolt, M., 2003. Influence of the Cu(In, Ga) Se2 thickness and Ga grading on solar cell performance. Prog. Photovolt. Res. Appl. 11, 77–88.

Lundberg, O., Edoff, M., Stolt, L., 2005. The effect of Ga-grading in CIGS thin film solar cells. Thin Solid Films. 520. http://dx.doi.org/10.1016/j.tsf.2004.11.080. 480–481.

Metz, A., et al., 2014. Industrial high performance crystalline silicon solar cells and modules based on rear surface passivation technology. Sol. Energy Mater. Sol. Cells 120, 417–425.

Nicollian, E.H., Brews, J.R., 1982. MOS (Metal Oxide Semiconductor) Physics and Technology. Wiley, New York.

Poncelet, O., Kotipalli, R., Vermang, B., Macleod, A., Francis, L.A., Flandre, D., 2017. Optimization of rear reflectance in ultra-thin CIGS solar cells towards > 20% efficiency. Sol. Energy 146, 443–452. http://dx.doi.org/10.1016/j.solener.2017.03.001.

Press release: Swedish solar energy expert Midsummer slashes CIGS layer thickness by half for reduced manufacturing cost, Stockholm, – Nov 25, 2014, midsummer.se/accounts/14232/files/207.pdf.

Press release: Solar Frontier Achieves World Record Thin-Film Solar Cell Efficiency: 22.3%, Tokyo – 8th December, 2015 < http://www.solar-frontier.com/eng/news/2015/C051171.html > .

Press release: Trina Solar Announces Achievement of 21.1% Average Efficiency for Industrially-Produced Monocrystalline PERC Cells, China– 4th July 2016, < http://www.trinasolar.com/us/news/trina-solar-announces-achievement-211-average-efficiency-industrially-produced-monocrystalline > .

Reinhard, P., Chirilă, A., Blösch, P., Pianezzi, F., Nishiwaki, S., Buechelers, S., Tiwari, A.N., 2013. Review of progress toward 20% efficiency flexible CIGS solar cells and manufacturing issues of solar modules. IEEE J. Photovolt 3, 572–580.

Schmidt, J., Merkle, A., Brendel, R., M vande Sanden, M.C., Kessels, W.M.M., 2008. Surface passivation of high-efficiency silicon solar cells by atomic-layer-deposited Al2 O3. Res. Appl. 16, 461–466.

Shockley, W., Read, W.T., 1952. Statistics of the recombinations of holes and electrons. Phys. Rev. 87, 835. http://dx.doi.org/10.1103/PhysRev. 87.835.

Song, J., Li, S.S., Huang, C.H., Crisalle, O.D., Anderson, T.J., 2004. Device modeling and simulation of the performance of Cu(In1-x, Gax)Se2 solar cells. Solid-State Electron. 48 (1), 73–79.

Trompoukis, C., Abdo, I., Cariou, R., Cosme, I., Chen, W., Deparis, O., Dmitriev, A., Drouard, E., Foldyna, M., Garcia-Caurel, E., Gordon, I., Heidari, B., Herman, A., Lalouat, L., Lee, K.-D., Liu, J., Lodewijks, K., Mandorlo, F., Massiot, I., Mayer, A., Mijkovic, V., Muller, J., Orobtchouk, R., Poulain, G., Prod'Homme, P., Roca i Cabarrocas, P., Seassal, C., Poortmans, J., Mertens, R., El Daif, O., Depauw, V., 2015. Photonic nanostructures for advanced light trapping in thin crystalline silicon solar cells. Phys. Status Sol. A 212 (1), 140–155. http://dx.doi.org/10.1002/pssa.201431180.

van Lare, C., Yin, G., Polman, A., Schmid, M., 2015. Light coupling and trapping in ultrathin Cu(In, Ga)Se2 solar cells using dielectric scattering patterns. ACS Nano 9 (10), 9603–9613.

Vermang, B., Fjällström, V., Pettersson, J., Salomé, P., Edoff, M., 2013. Sol. Energy Mater. Sol. Cells 117, 505–511. http://dx.doi.org/10.1016/j.solmat.2013.07.025.

Vermang, B., Wätjen, J.T., Fjällström, V., Rostvall, F., Edoff, M., Kotipalli, R., Henry, F., Flandre, D., 2014. Employing Si solar cell technology to increase efficiency of ultra-thin Cu(In, Ga)Se2 solar cells. Prog. Photovoltaics Res. Appl. 22 (10), 1023–1029. http://dx.doi.org/10.1002/pip.2527.

Vermang, B., Fjällström, V., Gao, X., Edoff, M., 2014. Improved rear surface passivation of Cu(In, Ga)Se2 solar cells: a combination of an Al_2O_3 rear surface passivation layer and nanosized local rear point contacts. IEEE J. Photovolt. 4 (1), 486–492. http://dx.

doi.org/10.1109/JPHOTOV.2013.2287769.

Vermang, B., Wätjen, J.T., Frisk, C., Fjällström, V., Rostvall, F., Edoff, M., Salomé, P., Borme, J., Nicoara, N., Sadewasser, S., 2014a. Introduction of Si PERC rear contacting design to boost efficiency of Cu(In, Ga)Se2 solar cells. IEEE J Photovolt. 4 (6), 1644–1649. http://dx.doi.org/10.1109/JPHOTOV.2014.2350696.

Vermang, B., Wätjen, J.T., Fjällström, V., Rostvall, F., Edoff, M., Gunnarsson, R., Pilch, I., Helmersson, U., Kotipalli, R., Henry, F., Flandre, D., 2014b. Thin Solid Films 582, 300.

Zhao, J., Wang, A., Green, M.A., Ferrazza, F., 1998. Novel 19.8% efficient “honeycomb” textured multicrystalline and 24.4% monocrystalline silicon solar cells. Appl. Phys. Lett. 73, 1991–1993.